High-pressure synthesis and Sn valence state analysis of $BaTiO_3$–SnO solid solution

Shoichiro Suzuki[a)]
Department of Crystalline Materials Science, Nagoya University, Nagoya 464-8603, Japan; and Murata Manufacturing, Co., Ltd., Nagaokakyo, Kyoto 617-8555, Japan

Ken Niwa
Department of Crystalline Materials Science, Nagoya University, Nagoya 464-8603, Japan

Atushi Honda
Murata Manufacturing, Co., Ltd., Nagaokakyo, Kyoto 617-8555, Japan

Shunsuke Muto
EcoTopia Science Institute, Nagoya University, Nagoya 464-8603, Japan

Akira Ando
Murata Manufacturing, Co., Ltd., Nagaokakyo, Kyoto 617-8555, Japan

Masashi Hasegawa
Department of Crystalline Materials Science, Nagoya University, Nagoya 464-8603, Japan

(Received 11 April 2014; accepted 24 September 2014)

$BaTiO_3$–SnO solid solutions have been investigated from the viewpoints of synthesis and Sn ion valence. First-principles calculations show that the solution energy of Sn^{2+} into the Ba sites in $BaTiO_3$ is less than that into the Ti sites under high pressure. The $BaTiO_3$–SnO solid solutions have been synthesized under high pressure (~20 GPa) and temperatures using a laser-heated diamond anvil cell. The synthesized materials have been characterized using x-ray diffractometry, scanning transmission electron microscopy, and energy-dispersive x-ray spectroscopy. It is found from these various methods that we have successfully synthesized uniform solid solutions of $BaTiO_3$–SnO. Furthermore, it is also clarified by the Sn L_3-edge electron energy loss spectra measurements that the valences of the Sn ions in the $BaTiO_3$–SnO solid solution are 2+. These results indicate that the Sn^{2+} ions are substituted into the Ba sites, according to the ion size. Consequently, the Sn ions can be substituted into the Ba sites of the shrinking $BaTiO_3$ lattice under high pressure, which is similar to the Ca and Sn co-substitution into Ba sites under ambient pressure as reported previously.

I. INTRODUCTION

Materials with high dielectric constants and low loss suitable for use over wide frequency and temperature ranges are desired for electronic applications[1] such as multilayered ceramic capacitors.[2] Barium titanate ($BaTiO_3$) is the most widely used ferroelectric material for this application.[3–7] However, its ferroelectric transition temperature (T_c) is nearly 125 °C, and its dielectric constant rapidly decreases above 125 °C following the Curie–Weiss law. It was reported that only the $PbTiO_3$–$BaTiO_3$ solid solution increases the T_c of $BaTiO_3$ and improves its ferroelectric property.[8] The Pb^{2+} ion has a 6*p* empty orbital, which mixes with the O^{2-} 2*p* in $PbTiO_3$ perovskites, leading to the formation of an asymmetric electric density at the top of the valence band.[9] This asymmetrical Pb–O bond distorts the oxygen octahedron so that it induces a large ferroelectric property and high T_c.[10]

In recent years, some first-principles calculation studies have predicted that $SnTiO_3$ would present excellent ferroelectric properties comparable to those of $PbTiO_3$ (Refs. 11 and 12) because the electron configuration of Sn^{2+} is similar to that of Pb^{2+}. Therefore, it is expected that the T_c and ferroelectric property of $BaTiO_3$ will be improved if the $BaTiO_3$–SnO solid solution could be synthesized. However, no studies have yet reported an increase in the T_c of a $BaTiO_3$–SnO solid solution.[13,14] It seems that the Sn^{2+} barely substitutes into the Ba sites because the Sn^{2+} ion has a smaller radius than the Ba ion.[12]

In comparison, we have discovered that the T_c of $BaTiO_3$ can be increased by Sn and Ca co-doping.[15–17] It was also found that this T_c increase was because of substituting Sn^{2+} into the Ba sites in the (Ba,Ca)TiO_3.[18] Because Ca doping decreases the lattice size because of its ion radius being smaller than that of Ba, it was

[a)]Address all correspondence to this author.
e-mail: shoichiro_suzuki@murata.co.jp
DOI: 10.1557/jmr.2014.293

 © Materials Research Society 2014

https://doi.org/10.1557/jmr.2014.293 Published online by Cambridge University Press

suggested that the decreased lattice size would be effective for substituting Sn^{2+} into the Ba sites. However, it was hard to distinguish whether the effects were due to a decreased lattice size or the Ca ion doping effects.

In this study, we have attempted to dope Sn^{2+} into the Ba sites using a high-pressure synthesis instead of the Ca co-doping at ambient pressure because the lattice size of $BaTiO_3$ decreases effectively under high pressure.[19] Moreover, the materials never evaporate, and the outside air never contacts the sample in this high-pressure synthesis. Thus, high-pressure synthesis has great advantages for not only preventing Sn evaporation but also for controlling the Sn valence, although the sample becomes too small (~100 μm) to measure these electric properties. Therefore, it can be clarified fundamentally that the Sn^{2+} ions are substituted into the Ba sites of the shrinking $BaTiO_3$ lattice using high-pressure synthesis.

First, the solution energies of substituted Sn^{2+} into the Ba and Ti sites in $BaTiO_3$ were estimated using a first-principles calculation. Then, on the basis of the calculated results, the $BaTiO_3$–SnO solid solutions have been synthesized at ~20 GPa and ~1500 K using a laser-heated diamond anvil cell (LH-DAC), which easily provides the range of high temperature and high pressure necessary for synthesizing compounds.[20] After synthesis, samples were analyzed using x-ray diffraction (XRD), scanning transmission electron microscopy (STEM), energy-dispersive x-ray spectroscopy (EDS), and electron energy loss spectroscopy (EELS) to analyze the solubility and valence states of the Sn ions in the synthesized solid solutions and confirm the substitution of Sn^{2+} into the Ba sites.

II. METHODS

A. Calculations

First-principles calculations were carried out by the Vienna ab-initio simulation package (VASP),[21] which is based on density functional theory (DFT). Generalized gradient approximation (GGA)[22] including spin polarization was used to determine the exchange–correlation energy. A plane-wave basis set with a cutoff energy of 500 eV was used. Atomic potentials were calculated using the projector augmented wave (PAW)[23] method. A 3 × 3 × 3 supercell of cubic $BaTiO_3$ with a perovskite structure was used. Moreover, a 2 × 2 × 2 *k*-point mesh was used in the reciprocal space. The local structural relaxation of the atomic positions around Sn^{2+} was allowed up to the second-nearest-neighbor atoms. In this study, we carefully compared the solution energies (E_{sol}) of Sn^{2+} at the Ba sites (Sn_{Ba}^{2+}) and the Ti sites (Sn_{Ti}^{2+}) as a function of their pressure on each other. Further details about the calculation methods were presented in our previous papers.[24,25]

B. Experiments

The raw ceramic materials SnO and $Ba_{0.96}TiO_{2.96}$ were used as starting materials. $Ba_{0.96}TiO_{2.96}$ was selected in consideration that the reported solubility limit of TiO_2 in $BaTiO_3$ was ~4 mol%.[26] These were weighed and mixed to realize a composition of $(Ba_{0.95}Sn_{0.05})Ti_{0.99}O_{2.98}$. The composition also considers that the maximum amount of Sn and the reported solubility limit of BaO in $BaTiO_3$ was ~1 mol%.[26] Then, the mixed powders were ball milled and dried. A LH-DAC with 450-μm culet size diamond anvils was used for synthesis experiments under high pressure and temperature. A plate of the mixed powder was sandwiched between hexagonal boron nitride (h-BN) or KCl pellets. Then, the sample was loaded in the sample chamber along with ruby chips as pressure markers. The pressure was determined from the shift of the ruby fluorescence spectrum at room temperature.[27] The sample was compressed to ~20 GPa at room temperature, and then a fiber laser was used to irradiate the sample from one side through the diamond anvil. Although the synthesis temperature was not measured directly in this study, the sample temperature could be estimated at ~1500 K because of the low thermal radiation from the heated spot. After laser heating for ~5 min at~20 GPa, the sample was quenched to room temperature by stopping the laser irradiation. The schematic illustrations of the DAC and laser system in this study are shown in Fig. 1.

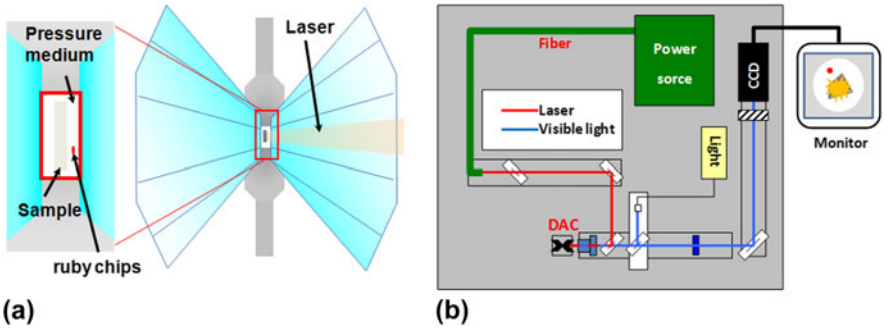


FIG. 1. Schematic illustrations of the diamond anvil cell and the laser heating system. (a) Sample chamber and diamond anvil cell and (b) full system of the LH-DAC for material synthesis under high pressure and temperature.

https://doi.org/10.1557/jmr.2014.293 Published online by Cambridge University Press

The crystalline phases of the recovered sample were analyzed and identified using the powder XRD technique. The composition of the recovered sample was analyzed by STEM (JEOL JEM-2200FS, JEOL Ltd., Tokyo, Japan) and EDS (JEOL JED-2300T, JEOL Ltd., Tokyo, Japan). The samples for the STEM measurements were fabricated using a focused ion beam lift-out method. The valence state of Sn in the recovered sample was determined by EELS (JEOL JEM-1000K RS equipped with a Gatan GIF Quantum equivalent) corresponding to the Sn $L_{2,3}$ edge. It was operated at room temperature with an accelerating voltage of 1000 kV.

III. RESULTS AND DISCUSSION

The pressure effects on the E_{sol} of Sn^{2+} in the $BaTiO_3$ are reported from DFT studies. Figure 2 shows the relationships among the pressure, the E_{sol} of Sn_{Ba}^{2+}, and Sn_{Ti}^{2+} in cubic $BaTiO_3$ perovskites estimated from first-principles calculations. Note that the E_{sol} of the Sn_{Ba}^{2+} is larger than that of the Sn_{Ti}^{2+} at ambient pressure. In Fig. 2, it is found that the E_{sol} of the Sn_{Ba}^{2+} decreases slightly initially with increasing pressure and then increases slightly, whereas that of the Sn_{Ti}^{2+} increases monotonically. Consequently, the E_{sol} of the Sn_{Ba}^{2+} is smaller than that of the Sn_{Ti}^{2+} under high pressures above ~1 GPa, and it is smallest at ~15 GPa. Furthermore, the E_{sol} difference between the Sn_{Ba}^{2+} and Sn_{Ti}^{2+} becomes larger with increasing pressure. This means that the Sn^{2+} prefers the Ba sites to the Ti sites as a substitution site with increasing pressure. Based on these calculations, we tried to synthesize a $BaTiO_3$–SnO solid solution at ~20 GPa.

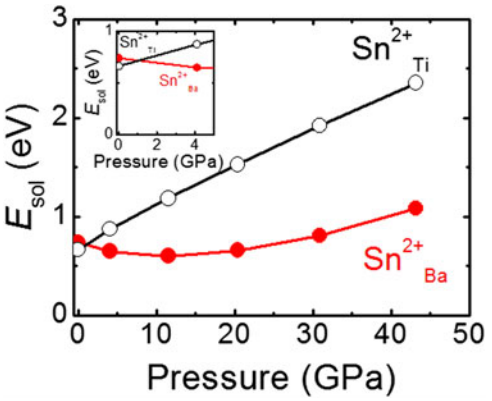


FIG. 2. Relationship between pressure and solution energies of Sn^{2+} at the Ba (Sn_{Ba}^{2+}) and Ti sites (Sn_{Ti}^{2+}) in the cubic $BaTiO_3$ estimated using first-principles calculations. The inset shows the relationship across the low-pressure region.

Figure 3 shows the photographs of the sample chamber at ~20 GPa before and after laser heating. It is found that the sample diameters are about 100 μm. A large difference of the sample shape before and after laser heating was not observed, suggesting that the sample did not melt during laser heating.

The recovered sample after laser heating was characterized by XRD. Figure 4 shows the XRD patterns measured at ambient pressure before and after laser heating at ~20 GPa. It was found that a SnO peak at ~30°, which is clearly observed before the laser heating, disappeared after the laser heating, although distinguishable changes were not observed in the pattern of the $BaTiO_3$ phase. In addition, it should be mentioned that no Sn or SnO_2 peaks are detected in the XRD patterns after laser heating, and BaO or TiO_2 peaks were also not detected. These results strongly suggest that the SnO reacts with $BaTiO_3$, and additionally, the Sn ions are substituted into vacancy sites of the $Ba_{0.96}TiO_{2.96}$ under high pressure and temperature.

The microstructure of the synthesized sample was examined to confirm the reaction between the $BaTiO_3$ and the SnO. Figure 5 shows the STEM image and the EDS distribution maps of Ba and Sn in the sample after laser heating at ~20 GPa. It is found that the Sn is distributed almost uniformly in the sample. It should be noted that Sn is detected at the same positions as Ba in the EDS distribution maps. The quantitative EDS analyses indicated by the red arrow in Fig. 5(a) are summarized in Table I. Note that these data from the EDS

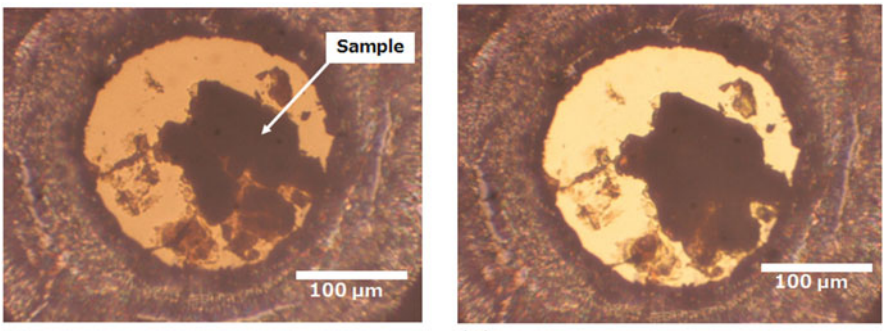


FIG. 3. Photographs of the sample chamber in the DAC at room temperature (a) before laser heating at ~20 GPa and (b) after laser heating at ~20 GPa.

https://doi.org/10.1557/jmr.2014.293 Published online by Cambridge University Press

analyses have an error of less than 5%. It is found that nearly identical amounts of Sn are detected at all points. Likewise, the Ba and Ti are also simultaneously detected at all points. In addition, the amount of Ti is shown to be greater than that of Ba, although this is not significant, taking in account the 5% error in the EDS spectra. As mentioned above, the XRD analysis indicates that the laser-heated sample comprises a single $BaTiO_3$ phase. Accordingly, it is concluded that the SnO has reacted with the $BaTiO_3$ and that the Sn is uniformly distributed in the $BaTiO_3$ phase, indicating the formation of a solid solution of $BaTiO_3$–SnO. Moreover, it is also suggested that the Sn ions are substituted into vacancy sites of the $Ba_{0.96}TiO_{2.96}$.

Finally, the valence state of the Sn ions in the synthesized sample has been determined by its EEL spectra to identify the Sn substitution site in the $BaTiO_3$. The Sn *M* edge is usually used to determine the Sn valence[28]; however, it is difficult to determine the valence of the Sn in the $BaTiO_3$ using the Sn *M* edge because its energy is close to that of the Ti *L* edge. Accordingly, we thus attempted to analyze the Sn *L* edge. The difference between the Sn L_3-edge energy of SnO and SnO_2 has been previously reported in a study using x-ray absorption fine structure.[29] From this report, it is known that SnO shows a 5 eV chemical peak shift from SnO_2. Figure 6 shows the EEL spectra corresponding to the Sn *L* edge of the $BaTiO_3$–SnO solid solution sample after laser heating at ~20 GPa. It is found that 4 peaks are observed at 3958, 4051, 4187, and 4477 eV around the *L* edge. The 3 peaks denoted with the letters L_1, L_2, and L_3 in Fig. 6 are assigned to the Sn *L* edge, according to the previous report.[29] Thus, it is found that the peak indicated with the arrow is unknown. Searching the literature for the unknown peak, we found that this peak is the Ca *K*-edge.[30] Accordingly, we have compared a cross section of Ca EEL spectra with that of Sn to calculate the ratio of the Ca quantity against the Sn quantity. As a result, it was found that the amount of Ca is about 5% against that of Sn, i.e., $(Ba_{0.95}Sn_{0.05}Ca_{0.0025})Ti_{0.99}O_{2.98}$. A small amount of Ca hardly affects Sn substitution as shown from our previous report.[15] Therefore, this estimation provides the conclusion that the Ca is an impurity and will not affect our results. Fortunately, the peak of the Ca *K*-edge becomes the reference of the Sn *L*-edge peak position. It was known that the peak position of the Ca *K*-edge is 4051 eV, determined from the previous report.[30] The Ca *K*-edge position provides the Sn L_1, L_2, and L_3 edges at 3958, 4187, and 4477 eV, respectively. Hence, the Sn L_1-, L_2-, and L_3-edge positions indicate that the valence state of the Sn in the sample is 2+, i.e., Sn^{2+}. If Sn were 4+, the Ca *K*-edge position would be 4056 eV, but this energy is unlikely for the Ca *K*-edge.

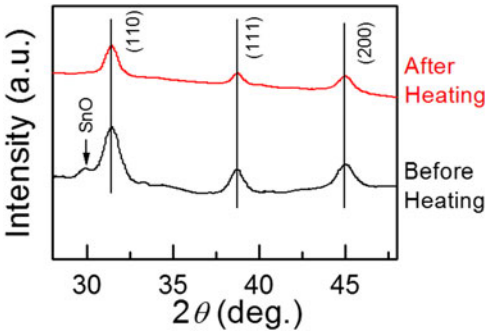


FIG. 4. The XRD pattern of the $BaTiO_3$–SnO sample before and after laser heating. The arrow indicates a main diffraction peak of SnO. Vertical lines indicate the (110), (111), and (200) peak positions of $BaTiO_3$ before laser heating.

Sn^{2+} ions are too large to substitute into the Ti sites.[11] Accordingly, if all Sn^{2+} are substituted into Ti sites, the lattice constant of $BaTiO_3$ would be increased. However, distinguishing changes are not observed in the pattern of the $BaTiO_3$ phase before and after laser heating as shown in Fig. 4. Moreover, the TiO_2 peak was not detected. It is evident that the Sn^{2+} is barely substituted into the Ti site and that instead the Sn^{2+} is substituted into the vacant Ba sites. Thus, the existence of Sn^{2+} allows us to conclude that almost all of the Sn^{2+} ions are substituted into the Ba sites of the $BaTiO_3$ in the synthesized sample. This also indicates that the high-pressure synthesis, which decreases the $BaTiO_3$ lattice, is effective for Sn

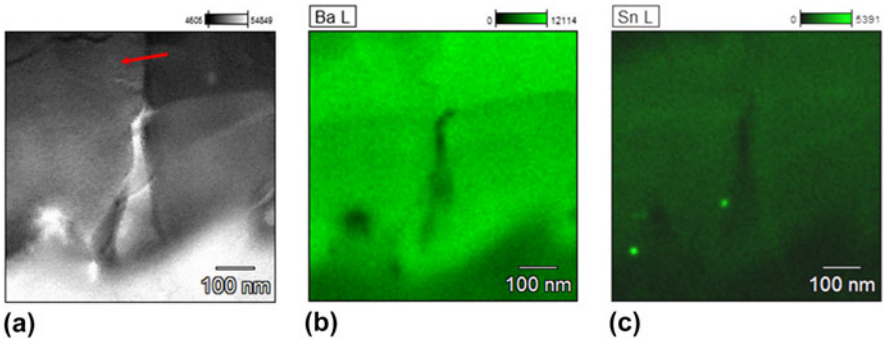


FIG. 5. STEM-EDS analysis results of the $BaTiO_3$–SnO sample after laser heating at ~20 GPa. (a) STEM image. The red arrow indicates the EDS analysis line. (b and c) EDS distribution maps: (b) Ba, (c) Sn.

https://doi.org/10.1557/jmr.2014.293 Published online by Cambridge University Press

TABLE I. Compositions obtained from the EDS data at the position indicated by the red arrow in Fig. 5(a). Note that these data from the EDS analyses have an error of less than 5%.

Distance (nm)	Ti (at.%)	Sn (at.%)	Ba (at.%)
14	55	4	41
29	55	4	41
43	54	3	43
57	54	3	43
72	55	3	42
86	56	3	41
100	56	3	41

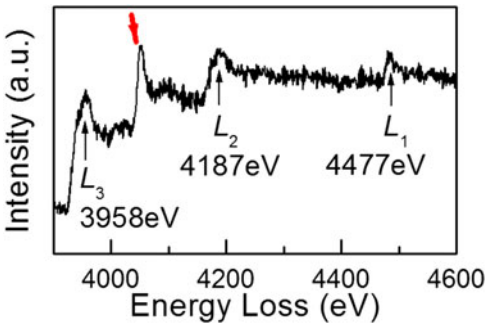


FIG. 6. EEL spectra corresponding to the Sn L edge of the $BaTiO_3$–SnO sample after laser heating at ~20 GPa. Arrows indicate the L_3, L_2, and L_1 peak positions and unknown peak.

substitution into the Ba site, as well as the reported Ca co-doping. Therefore, it is concluded that decreasing the lattice size of $BaTiO_3$ is effective for substituting Sn into the Ba sites. Besides, this consideration is consistent with the calculation results mentioned above which indicate that the Sn prefers substituting into the Ba sites rather than the Ti sites under high pressure.

IV. CONCLUSIONS

Formation of $BaTiO_3$–SnO solid solutions has been investigated by solution energy calculations, high-pressure synthesis, and Sn valence characterization. The first-principles calculations of the solution energy show that the Sn^{2+} ions are preferentially substituted into the Ba sites in $BaTiO_3$ under high pressure rather than into the Ti sites. Then, on the basis of the calculated results, $BaTiO_3$–SnO solid solutions have been synthesized under high pressure (~20 GPa) and high temperature (~1500 K) using the LH-DAC. The synthesized solid solutions have been characterized using XRD, STEM, and EDS. It is found from these methods that the synthesized solid solution is of a single phase with a uniform composition. In addition, it is also clarified from the Sn L_3-edge EEL spectra that the valences of the Sn ions in the solid solution are 2+. These results indicate that the Sn^{2+} ions are substituted into Ba sites, according to the ion size. Consequently, the Sn ions can be substituted into the Ba sites of the shrinking $BaTiO_3$ lattice under high pressure, which is similar to the Ca and Sn cosubstitution into the Ba sites under ambient pressure reported previously.

REFERENCES

1. A.V. Hippel, R.G. Breckenridge, F.G. Chesley, and L. Tisza: High dielectric constant ceramics. *Ind. Eng. Chem.* **38**, 1097 (1946).
2. Y. Sakabe: Multilayer ceramic capacitors. *Curr. Opin. Solid State Mater. Sci.* **2**, 584 (1997).
3. H. Saito, H. Chazono, H. Kishi, and N. Yamaoka: X7R multilayer ceramic capacitors with nickel electrodes. *Jpn. J. Appl. Phys.* **30**, 2307 (1991).
4. N. Wada, H. Tanaka, Y. Hamaji, and Y. Sakabe: Microstructures and dielectric properties of fine-grained $BaTiO_3$ ceramics. *Jpn. J. Appl. Phys.* **35**, 5141 (1996).
5. J. Yamamatsu, N. Kawano, T. Arashi, A. Sato, Y. Nakano, and T. Nomura: Reliability of multilayer ceramic capacitors with nickel electrodes. *J. Power Sources* **60**, 199 (1996).
6. T. Nakamura, H. Sano, T. Konoike, and K. Tomono: $BaTiO_3$-based non-reducible low-loss dielectric ceramics. *Jpn. J. Appl. Phys.* **38**, 5457 (1999).
7. Y. Sakabe, Y. Hamaji, H. Sano, and N. Wada: Effects of rare-earth oxides on the reliability of X7R dielectrics. *Jpn. J. Appl. Phys.* **41**, 5668 (2002).
8. G. Burns: Lattice modes in ferroelectric perovskites. II. $Pb_{1-x}Ba_xTiO_3$ including $BaTiO_3$. *Phys. Rev. B* **10**, 1951 (1974).
9. D.J. Payne, R.G. Egdell, A. Walsh, G.W. Watson, J. Guo, P-A. Glans, T. Learmonth, and K.E. Smith: Electronic origins of structural distortions in post-transition metal oxides: Experimental and theoretical evidence for a revision of the lone pair model. *Phys. Rev. Lett.* **96**, 157403 (2006).
10. Y. Kuroiwa, S. Aoyagi, A. Sawada, J. Harada, E. Nishibori, M. Takata, and M. Sakata: Evidence for Pb-O covalency in tetragonal $PbTiO_3$. *Phys. Rev. Lett.* **87**, 217601 (2001).
11. S.F. Matar, I. Baraille, and M.A. Subramanian: First principles studies of $SnTiO_3$ perovskite as potential environmentally benign ferroelectric material. *Chem. Phys.* **355**, 43 (2009).
12. Y. Uratani, T. Shishidou, and T. Oguchi: First-principles study of lead-free piezoelectric $SnTiO_3$. *Jpn. J. Appl. Phys.* **47**, 7735 (2008).
13. Y. Xie, S. Yin, T. Hashimoto, H. Kimura, and T. Sato: Microwave-hydrothermal synthesis of nano-sized Sn^{2+}-doped $BaTiO_3$ powders and dielectric properties of corresponding ceramics obtained by spark plasma sintering method. *J. Mater. Sci.* **44**, 4834 (2009).
14. C.E. Lee, C.A. Randall, D.Y. Kim, and S.H. Kim: Multi-site and multi-ionization of Sn in the doping of $BaTiO_3$. *J. Am. Ceram. Soc.* **97**, 513 (2014).
15. S. Suzuki, T. Takeda, A. Ando, and H. Takagi: Ferroelectric phase transition in Sn^{2+} ions doped (Ba,Ca)TiO_3 ceramics. *Appl. Phys. Lett.* **96**, 132903 (2010).
16. S. Suzuki, T. Takeda, A. Ando, T. Oyama, N. Wada, H. Niimi, and H. Takagi: Effect of Sn^{2+} ion substitution on dielectric properties of (Ba,Ca)TiO_3 ferroelectric ceramics. *Jpn. J. Appl. Phys.* **49**, 09MC04 (2010).
17. S. Suzuki, A. Honda, S. Higai, A. Ando, N. Wada, and H. Takagi: Effects of lattice constant and sintering atmosphere on substitution of Sn^{2+} ions at Ba site in (Ba,Ca)TiO_3 perovskites: Experimental and theoretical studies. *Jpn. J. Appl. Phys.* **50**, 09NC11 (2011).

https://doi.org/10.1557/jmr.2014.293 Published online by Cambridge University Press

18. S. Suzuki, N. Iwaji, A. Honda, S. Higai, N. Wada, A. Ando, and H. Takagi: Substitution of Sn ions in (Ba,Ca)TiO_3 perovskites. *Jpn. J. Appl. Phys.* **51**, 09LC08 (2012).
19. G.A. Samara: Pressure and temperature dependence of the dielectric properties and phase transitions of the ferroelectric perovskites: $PbTiO_3$ and $BaTiO_3$. *Ferroelectrics* **2**, 277 (1971).
20. M. Hasegawa and T. Yagi: Growth of nitride crystals in a super-critical nitrogen fluid under high pressures and high temperatures yield using diamond anvil cell and YAG laser heating. *J. Cryst. Growth* **217**, 349 (2000).
21. G. Kresse: Efficient iterative schemes for ab initio total-energy calculations using a plane-wave basis set. *Phys. Rev. B* **54**, 11169 (1996).
22. J.P. Perdew, K. Burke, and M. Ernzerhof: Generalized gradient approximation made simple. *Phys. Rev. Lett.* **77**, 3865 (1996).
23. G. Kresse: From ultrasoft pseudopotentials to the projector augmented-wave method. *Phys. Rev. B* **59**, 1758 (1999).
24. S. Higai, A. Honda, Y. Motoyoshi, N. Wada, H. Takagi, and Y. Sakabe: Industry meets theory: Computational R & D for innovative products. *J. Phys.: Condens. Matter* **22**, 384209 (2010).
25. A. Honda, S. Higai, Y. Motoyoshi, N. Wada, and H. Takagi: Theoretical study on interactions between oxygen vacancy and doped rare-earth elements in barium titanate. *Jpn. J. Appl. Phys.* **50**, 09NE01 (2011).
26. S. Lee, C.A. Randall, and Z.K. Liu: Modified phase diagram for the barium oxide-titanium dioxide system for the ferroelectric barium titanate. *J. Am. Ceram. Soc.* **90**, 2589 (2007).
27. H.K. Mao, J. Xu, and P.M. Bell: Calibration of the ruby pressure gauge to 800 kbar under quasi-hydrostatic conditions. *J. Geophys. Res.* **91**, 4673 (1986).
28. M. Moreno, R. Egerton, and P. Midgley: Differentiation of tin oxides using electron energy-loss spectroscopy. *Phys. Rev. B* **69**, 233304 (2004).
29. Z. Liu, K. Handab, K. Kaibuchi, and Y. Tanaka, and J. Kawai: Comparison of the Sn L edge X-ray absorption spectra and the corresponding electronic structure in Sn, SnO, and SnO_2. *J. Electron Spectrosc. Relat. Phenom.* **135**, 155 (2004).
30. D.R. Neuville, L. Cormier, D. de Ligny, J. Roux, A-M. Flank, and P. Lagarde: Environments around Al, Si, and Ca in aluminate and aluminosilicate melts by X-ray absorption spectroscopy at high temperature. *Am. Mineral.* **93**, 228 (2008).

https://doi.org/10.1557/jmr.2014.293 Published online by Cambridge University Press